Surface Science 604 (2010) 2139–2149

Contents lists available at ScienceDirect

Surface Science

journal homepage: www.elsevier.com/ locate/susc

Scanning tunneling spectroscopic evidence of crossover transition in the two-impurity Kondo problem

Emi Minamitani, Wilson Agerico Diño, Hiroshi Nakanishi, Hideaki Kasai *

Department of Precision Science & Technology and Applied Physics, Osaka University, 2-1 Yamadaoka, Suita, Osaka 565-0871, Japan

ARTICLE INFO

Article history:
Received 11 June 2010
Accepted 7 September 2010
Available online 16 September 2010

Keywords:
Metal surface
Scanning tunneling spectroscopy
Numerical renormalization group
Two-impurity Kondo effect

ABSTRACT

To explore the crossover transition in the two-impurity Kondo problem, we calculate the differential conductance (dI/dV) corresponding to scanning tunneling spectroscopy (STS) measurements of a magnetic dimer adsorbed on a metal surface covered by a decoupling layer. With the aid of the numerical renormalization group (NRG) technique, we find that the peak structure of the dI/dV spectra near the Fermi level changes gradually as a function of the adatom separation and the coupling between the adatom localized spins and the metal surface conduction band. When the coupling becomes small, the peak disappears and, instead, a dip structure appears near the Fermi level. This dip structure is the manifestation of the strong antiferromagnetic correlation between the localized spins. We conclude that the gradual change of the dI/dV structure from a peak structure to a dip structure is an evidence of the crossover transition in the two-impurity Kondo problem.

© 2010 Elsevier B.V. All rights reserved.

1. Introduction

The Kondo effect is originally found as the existence of resistance minimum in dilute magnetic alloy [1]. In such system, the interaction between the metal conduction electron and localized spin in the magnetic atom results in formation of so-called "Yosida–Kondo singlet", the singlet state between the localized spin and the conduction electrons [2]. In recent years, with the advent of scanning tunneling spectroscopy (STS), it becomes possible to detect the formation of the local Yosida–Kondo singlet on solid surfaces with high spacial resolution. The Yosida–Kondo singlet appears as a sharp peak structure near the Fermi level (Yosida–Kondo peak) in STS spectra. This STS observation of the Kondo effect has been extensively investigated for a single magnetic atom on a metal surface [3–12].

When two magnetic atoms are placed on a metal surface, not only the Kondo effect, but also the Ruderman–Kittel–Kasuya–Yosida (RKKY) interaction [13] plays an important role. The interference between the Kondo effect and the spin-ordering effect of the RKKY interaction gives rise to the "two-impurity Kondo problem". This two-impurity Kondo problem has long been investigated [14–19]. Generally, the low temperature physics depends on the ratio between the RKKY coupling constant J_{RKKY} and the one-impurity Kondo temperature T_K [14]. In the limit of strong ferromagnetic RKKY coupling ($-J_{RKKY} \gg T_K$), a two stage Kondo effect occurs: When temperature T gets smaller than $|J_{RKKY}|$, the two localized spins are locked ferromagnetically into a spin-triplet state described by an effective spin $S=1$. With further reduction of T, screening of the effective spin $S=1$ arises. In the two-impurity case, the localized spins interact with two conduction channels characterized by even and odd parity. The coupling between the localized spins and each conduction channel is parity dependent and the screening process has two stages. First, the effective $S=1$ is partially compensated to effective $S=1/2$, and then completely suppressed as T goes to zero [14]. In the limit of strong antiferromagnetic RKKY coupling ($J_{RKKY} \gg T_K$), the localized spins are locked into a spin singlet state (the antiferromagnetic region), and the Kondo effect plays a minor role. In the $T_K \gg |J_{RKKY}|$ region (the Kondo region), the RKKY interaction plays a minor role.

The scenarios in the corresponding limits are very reasonable, but the physics in the region at intermediate values of J_{RKKY} is nontrivial. The numerical renormalization group (NRG) studies on the electron-hole (e-h) symmetric Hamiltonian found that a critical point separates the Kondo region and the antiferromagnetic region [15,16]. However, it is now apparent that the critical point results from the e-h symmetry of the model Hamiltonian [17,18]. In general, e-h symmetry is broken (e.g., energy dependence in tunneling matrix elements) and the quantum phase transition is replaced by a crossover transition [19]. However, the existence of the crossover transition had never been observed experimentally, and the manner of the transition in realistic materials is still an open question.

The scanning tunneling spectroscopy (STS) observation of a magnetic dimer on a nonmagnetic metal surface would provide a great opportunity to unravel the physics of the crossover transition in the two-impurity Kondo problem. Recently, Wahl et al. showed that

* Corresponding author. Tel.: +81 6 6879 7857; fax: +81 6 6879 7859.
E-mail address: kasai@dyn.ap.eng.osaka-u.ac.jp (H. Kasai).

0039-6028/$ – see front matter © 2010 Elsevier B.V. All rights reserved.
doi:10.1016/j.susc.2010.09.005

the Yosida–Kondo peak for Co dimer on Cu(100) surface varies with the adatom separation [20]. In our earlier studies, we modeled the STS observation and derived the formula of the STS spectra with the aid of the Keldysh Green function method. The STS spectra are calculated by the numerical renormalization group (NRG) technique and we confirmed that the ferromagnetic (antiferromagnetic) RKKY interaction tends to sharpen (broaden) the peak structure of STS spectra in such system [21,22]. Our results are in good agreement with the other theoretical study using the NRG technique [23].

The main purpose of this work is to explore the evidence of the crossover transition within the STS spectra. To explore the crossover transition from the Kondo region to the antiferromagnetic region, we need to realize $J_{RKKY} \gg T_K$ situation. Both J_{RKKY} and T_K strongly depend on the ratio between the Coulomb interaction U and the coupling between the adatom spins and the metal surface conduction band Γ. As schematically shown in Fig. 1, T_K decays much faster than J_{RKKY} as Γ decreases. With small Γ, we would expect that the antiferromagnetic RKKY interaction becomes dominant at a particular adatom separation. For this reason, we calculate the dI/dV spectra for several values of Γ and the adatom separation.

2. Model and method

2.1. Model Hamiltonian

As experiments show [8,24,25], Γ can be suppressed by covering the metal surface with a decoupling layer, which leads to decrease in T_K and makes the RKKY interaction dominant. In the present study, we consider the model system shown in Fig. 2.

Magnetic atom 2 is located at a distance of a Å with respect to magnetic atom 1. We assume that the center of atom 1 is located at $\mathbf{R}_1 = (a/2, 0, R_m)$ Å and that of atom 2 is located at $\mathbf{R}_2 = (-a/2, 0, R_m)$ Å. R_m is the radius of adatom. We set $R_m = 0.4$ Å [11]. The STM tip apex is at a distance of z_p from the metal surface, directly above atom 1. R_o is the thickness of the decoupling layer and we set $R_o = 5$Å. The corresponding model Hamiltonian is given by

$$\begin{aligned} H &= H_{A2} + H_{tip} + H_{mix} \\ &= \sum_{i\sigma} E_d d^\dagger_{i\sigma} d_{i\sigma} + \sum_{k,\sigma} E_k c^\dagger_{k\sigma} c_{k\sigma} + \sum_{ik\sigma} \left(V_{kdi} c^\dagger_{k\sigma} d_{i\sigma} + h.c. \right) \\ &\quad + \sum_i U n_{i\uparrow} n_{i\downarrow} + \sum_{p,\sigma} E_p c^\dagger_{p\sigma} c_{p\sigma} \\ &\quad + \sum_{pi\sigma} \left(T_{pdi} c^\dagger_{p\sigma} d_{i\sigma} + h.c. \right) + \sum_{pk\sigma} \left(W_{pk} c^\dagger_{p\sigma} c_{k\sigma} + h.c. \right). \end{aligned} \tag{1}$$

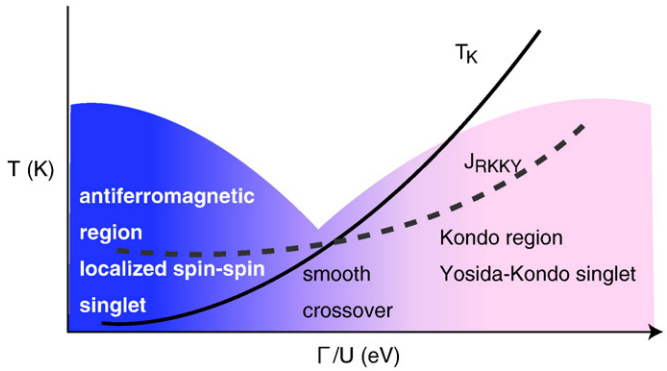

Fig. 1. Diagram of the smooth crossover in the two-impurity Kondo effect. T is the temperature. T_K is the Kondo temperature and J_{RKKY} is the RKKY coupling constant.

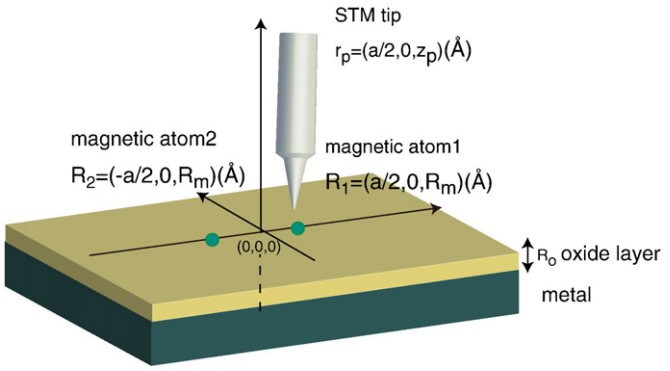

Fig. 2. STS observation of a magnetic dimer on a nonmagnetic metal surface. Distances between the adatoms (a), the tip apex and the metal surface (z_p) are given in Ångströms (Å). STM tip is placed directly above atom 1.

Here $d^\dagger_{i\sigma}$, $c^\dagger_{k\sigma}$ and $c^\dagger_{p\sigma}$ correspond to creation operators for adatom d electrons, metal surface conduction electrons, and tip electrons with spin σ, respectively. $n_{i\sigma} = d^\dagger_{i\sigma} d_{i\sigma}$. E_d, E_k and E_p correspond to the energies of adatom d electrons, conduction electrons and tip electrons, respectively. Adatom index $i = 1,2$. k corresponds to the metal surface electron wavenumber, and p corresponds to eigenstate quantum number of the STM tip electrons. T_{pdi}, W_{pk}, and V_{kdi} correspond to the tip-adatom, tip-surface, and adatom–surface electron tunneling matrix elements, respectively. U gives the on-site Coulomb repulsion on adatoms. We approximate the coefficients in the Hamiltonian (1) as

$$V_{kd1} = V_0 exp(i\mathbf{k}\cdot a/2), V_{kd2} = V_0 exp(-i\mathbf{k}\cdot a/2), \tag{2}$$

$$W_{kp} = W_0 exp\left(-\left(z_p - R_s + R_o\right)/\lambda\right) exp\left(-i\left(\mathbf{k}\cdot\mathbf{r_p}\right)\right), \tag{3}$$

$$T_{pdi} = T_0 \frac{\psi_{di}\left(\mathbf{r_p} - \mathbf{R_i}\right)}{\psi_{di}(\mathbf{r_m} + \mathbf{R})} = T_0 \Phi_{di}, \tag{4}$$

and

$$\Phi_{di} = \frac{\psi_{di}\left(\mathbf{r_p} - \mathbf{R_i}\right)}{\psi_{di}(\mathbf{r_m} + \mathbf{R})}. \tag{5}$$

ψ_{di} corresponds to the d electron orbital of adatom i. In this study, we use the dz^2 orbital of Co as ψ_{di} [26].We approximate the tip apex as a nonmagnetic metal sphere whose center is positioned at $\mathbf{r_p} = \left(a/2, 0, z_p\right)$ with radius Rs. $\mathbf{r_m} = (0, 0, R_m)$ $\mathbf{R} = (0, 0, Rs)$, and $\mathbf{a} = (a, 0, 0)$. W_0 and T_0 correspond to the values of the tunneling matrix elements when the STM tip is in contact with the surface or adatoms, respectively. V_0 is the tunneling matrix element between a localized d electron and a metal surface in the single impurity case. Using these parameters and the density of state of the metal surface conduction electron (ρ_k), Γ is defined as $\Gamma = \pi\rho_k V_0^2$.

2.2. Expression of tunneling current and differential conductance

Based on the model Hamiltonian (1), we calculate the tunneling current from the STM tip to the surface. The tunneling current can be calculated from the time derivative of the occupation number of electrons at the STM tip.

$$I = -\frac{\partial}{\partial t} e \sum_{p,\sigma} < c^\dagger_{p\sigma}(t) c_{p\sigma}(t) > \tag{6}$$

By the equation of motion (EOM), Eq. (6) can be rewritten as:

$$\begin{aligned} I &= -e\frac{1}{i\hbar}\sum_{p,\sigma}<\left[c^{\dagger}_{p\sigma}(t)c_{p\sigma}(t),H(t)\right]> \\ &= \frac{ie}{\hbar}\left\{\sum_{p,i,\sigma}\left(T_{pdi}<c^{\dagger}_{p\sigma}(t)d_{i\sigma}(t)> -T_{dip}<d^{\dagger}_{i\sigma}(t)c_{p\sigma}(t)>\right)\right. \\ &\quad \left.+\sum_{p,k,\sigma}\left(W_{pk}<c^{\dagger}_{p\sigma}(t)c_{k\sigma}(t)> -W_{kp}<c^{\dagger}_{k\sigma}(t)c_{p\sigma}(t)>\right)\right\} \end{aligned} \tag{7}$$

From the definition of the Keldysh Green's function [11,27,28],

$$\begin{aligned} I &= \frac{e}{\hbar}\left\{\sum_{p,i,\sigma}\left(T_{pdi}G^{-+}_{d_ip\sigma}(0,0)-T_{dip}G^{-+}_{pd_i\sigma}(0,0)\right)\right. \\ &\quad \left.+\sum_{p,k,\sigma}\left(W_{pk}G^{-+}_{kp\sigma}(0,0)-W_{kp}G^{-+}_{pk\sigma}(0,0)\right)\right\} \\ &= -\frac{2e}{\hbar}\Re\left\{\sum_{p,i,\sigma}T_{dip}G^{-+}_{pd_i\sigma}(0,0)+\sum_{p,k,\sigma}W_{kp}G^{-+}_{pk\sigma}(0,0)\right\} \end{aligned} \tag{8}$$

The structure of the EOM for the Keldysh Green's function is the same for the equilibrium zero-temperature Green's function. Solving the EOM for the equilibrium zero-temperature Green's function, we obtain

$$\begin{aligned} G_{pd1\sigma}(t,t') &= \int dt_2 g^0_{pp\sigma}(t,t_2)T_{pd1}G_{d1d1\sigma}(t_2,t')+g^0_{pp\sigma}(t,t_2)T_{pd2}G_{d2d1\sigma}(t2,t') \\ &\quad +\iint dt_1dt_2\sum_k g^0_{pp\sigma}(t,t_2)W_{pk}g^0_{kk\sigma}(t,t_1)V_{kd1}G_{d1d1\sigma}(t_1,t') \\ &\quad +\sum_{k\sigma}g^0_{pp\sigma}(t,t_2)W_{pk}g^0_{kk\sigma}(t,t_1)V_{kd2}G_{d2d1\sigma}(t_1,t') \\ &\quad +\sum_{kp'\sigma}g^0_{pp\sigma}(t,t_2)W_{pk}g^0_{kk\sigma}(t,t_1)W_{kp'}G_{pd1\sigma}(t_1,t'), \end{aligned} \tag{9}$$

$$\begin{aligned} G_{pk\sigma}(t,t') &= \int dt_2 G_{pd1\sigma}(t,t_2)V_{kd1}g^0_{kk\sigma}(t_2,t')+G_{pd2\sigma}(t,t_2)V_{kd2}g^0_{kk\sigma}(t_2,t') \\ &\quad +\int dt_2 g^0_{pp}(t,t_2)W_{pk}g^0_{kk\sigma}(t_2,t') \\ &\quad +\iint dt_1dt_2\sum_{p\sigma}G_{pd1\sigma}(t,t_1)T_{d1p'}g^0_{p'p'\sigma}(t_1,t_2)W_{p'k}g^0_{kk\sigma}(t_2,t') \\ &\quad +G_{pd2\sigma}(t,t_1)T_{d2p'}g^0_{p'p'\sigma}(t_1,t_2)W_{p'k}g^0_{kk\sigma}(t_2,t') \\ &\quad +\sum_{k'p'\sigma}G_{pk'\sigma}(t,t_1)W_{p'k'}g^0_{p'p'\sigma}(t_1,t_2)W_{p'k}g^0_{kk\sigma}(t_2,t). \end{aligned} \tag{10}$$

We neglect 3rd and higher order terms in W_{pk} and T_{dip}, that is, we drop the last term of Eqs. (9) and (10). Using the Langreth theorem [28] and the Fourier transformation, the tunneling current can be rewritten as

$$\begin{aligned} I &= -\frac{2e}{h}\int d\omega\Re\left\{\sum_{p\sigma}T_{pd1}G^{<}_{pd1\sigma}(\omega)+T_{pd2}G^{<}_{pd2\sigma}(\omega)+\sum_{pk\sigma}W_{kp}G^{<}_{pk\sigma}(\omega)\right\} \\ &= -\frac{2e}{h}\left[\int d\omega\Re\left\{\sum_{p\sigma}T_{pd1}G^{<}_{pd1\sigma}(\omega)+T_{pd2}G^{<}_{pd2\sigma}(\omega)\right.\right. \\ &\quad +\sum_{pk\sigma}W_{kp}\left(G^{r}_{pd1\sigma}(\omega)V_{kd1}g^{0<}_{kk\sigma}(\omega)+G^{<}_{pd1\sigma}(\omega)V_{kd1}g^{0a}_{kk\sigma}(\omega)\right) \\ &\quad +\sum_{pk\sigma}W_{kp}\left(G^{r}_{pd2\sigma}(\omega)V_{kd2}g^{0<}_{kk\sigma}(\omega)+G^{<}_{pd2\sigma}(\omega)V_{kd2}g^{0a}_{kk\sigma}(\omega)\right) \\ &\quad +\sum_{pk\sigma}W_{kp}\left(g^{0r}_{pp}(\omega)W_{pk}g^{0<}_{kk\sigma}(\omega)+g^{0<}_{pp}(\omega)W_{pk}g^{0a}_{kk\sigma}(\omega)\right) \\ &\quad +\sum_{pp'ki\sigma}W_{kp}G^{r}_{pdi\sigma}(\omega)T_{dip'}g^{0r}_{p'p'\sigma}(\omega)W_{p'k}g^{0<}_{kk\sigma}(\omega) \\ &\quad +\sum_{pp'k\sigma}W_{kp}G^{r}_{pdi\sigma}(\omega)T_{dip'}g^{0<}_{p'p'\sigma}(\omega)W_{p'k}g^{0a}_{kk\sigma}(\omega) \\ &\quad \left.\left.+\sum_{pp'k\sigma}W_{kp}G^{<}_{pdi\sigma}(\omega)T_{dip'}g^{0a}_{p'p'\sigma}(\omega)W_{p'k}g^{0a}_{kk\sigma}(\omega)\right\}\right] \end{aligned} \tag{11}$$

As Eqs. (9) and (10), we drop the last three terms in Eq. (11) which include 3rd and higher order term in T_{dip} and W_{pk}.

Here,

$$\sum_{\mathbf{k}\sigma}exp(-i\mathbf{k}\cdot\mathbf{r})g^{0r}_{kk\sigma}=\sum_{\sigma}-i\pi\rho_kJ_0(k_Fr) \tag{12}$$

(J_0 is the 0th order Bessel function)

and,

$$g^{0<}_{kk\sigma}(\omega)=-2if_k(\omega)\Im g^{0r}_{kk\sigma}(\omega) \tag{13}$$

$$g^{0<}_{pp\sigma}(\omega)=-2if_p(\omega)\Im g^{0r}_{pp\sigma}(\omega) \tag{14}$$

(f_k and f_p are the Fermi distribution function for the metal surface and the STM tip, respectively.)

Inserting Eqs. (2)–(4) and (12)–(14), we obtain

$$\begin{aligned} I &= -\frac{2e}{h}\left[\int d\omega\Re\left\{\sum_{p\sigma}T_0\Phi_{d1}G^{<}_{pd1\sigma}(\omega)+T_0\Phi_{d2}G^{<}_{pd2\sigma}(\omega)\right\}\right. \\ &\quad -\sum_{pk\sigma}\pi\rho_kW_0V_0e^{-2(z-R_s)/\lambda}J_0\left(k_Fr_{p1}\right)\left(2f_k(\omega)\Im G^{r}_{pd1\sigma}(\omega)+\Im G^{<}_{pd1\sigma}(\omega)\right) \\ &\quad -\sum_{pk\sigma}\pi\rho_kW_0V_0e^{-2(z-R_s)/\lambda}J_0\left(k_Fr_{p2}\right)\left(2f_k(\omega)\Im G^{r}_{pd2\sigma}(\omega)+\Im G^{<}_{pd2\sigma}(\omega)\right) \\ &\quad \left.+\sum_{pk\sigma}2\pi^2\rho_k\rho_pW_0^2e^{-2(z-R_s)/\lambda}\left(f_k(\omega)-f_p(\omega)\right)\right]. \end{aligned} \tag{15}$$

Here, r_{p1} and r_{p2} are defined as $\sqrt{(R_{1x}-r_{px})^2+(R_{1y}-r_{py})^2}$ and $\sqrt{(R_{2x}-r_{px})^2+(R_{2y}-r_{py})^2}$, respectively. The Green's functions in Eq. (15) are expanded as:

$$\begin{aligned} G^{r}_{pdi\sigma}(\omega) &= T_0\Phi_{di}g^{0r}_{pp\sigma}(\omega)G^{r}_{didi\sigma}(\omega) \\ &\quad +T_0\Phi_{dj}g^{0r}_{pp\sigma}G^{r}_{djdi\sigma}(\omega) \\ &\quad -ijJ_{vw}\left(r_{pi}\right)g^{0r}_{pp\sigma}G^{r}_{didi\sigma}(\omega) \\ &\quad -ijJ_{vw}\left(r_{pj}\right)g^{0r}_{pp\sigma}G^{r}_{djdi\sigma}(\omega) \end{aligned} \tag{16}$$

$$\begin{aligned} G^{<}_{pdi\sigma}(\omega) &= T_0\Phi_{di}\{g^{0r}_{pp\sigma}(\omega)G^{<}_{didi\sigma}(\omega)-2if_p(\omega)\Im g^{0r}_{pp\sigma}(\omega)G^{a}_{didi\sigma}(\omega)\} \\ &\quad +T_0\Phi_{dj}\{g^{0r}_{pp\sigma}(\omega)G^{<}_{djdi\sigma}(\omega)-2if_p(\omega)\Im g^{0r}_{pp\sigma}(\omega)G^{a}_{djdi\sigma}(\omega)\} \\ &\quad -ijJ_{vw}\left(r_{pi}\right)g^{0r}_{pp\sigma}G^{<}_{didi\sigma}(\omega) \\ &\quad +2if_k(\omega)J_{vw}\left(r_{pi}\right)g^{0r}_{pp\sigma}G^{a}_{didi\sigma}(\omega) \\ &\quad +2if_p(\omega)J_{vw}\left(r_{pi}\right)\Im g^{0r}_{pp\sigma}G^{a}_{didi\sigma}(\omega) \\ &\quad -ijJ_{vw}\left(r_{pj}\right)g^{0r}_{pp\sigma}G^{<}_{djdi\sigma}(\omega) \\ &\quad +2if_k(\omega)J_{vw}\left(r_{pj}\right)g^{0r}_{pp\sigma}G^{a}_{djdi\sigma}(\omega) \\ &\quad +2if_p(\omega)J_{vw}\left(r_{pj}\right)\Im g^{0r}_{pp\sigma}G^{a}_{djdi\sigma}(\omega) \\ &\quad \times\left(J_{vw}(r)=\pi\rho_kJ_0(k_Fr)V_0W_0e^{(-(z-R_s)/\lambda)}\right) \end{aligned} \tag{17}$$

ρ_p gives the density of states of the STM tip electrons. We define $J_{vw}(r)$ as:

$$J_{vw}(r)=\pi\rho_kJ_0(k_Fr)V_0W_0exp\left(-\left(z_p-R_s+R_o\right)/\lambda\right). \tag{18}$$

Finally, we approximate the Keldysh lesser Green's function in Eq. (18) as:

$$G^{<}_{didi\sigma}(\omega) = -2if_k(\omega)\Im G^r_{djdi}(\omega). \tag{19}$$

The reason is that our target is very small bias region (−0.01–0.01 V). The bias voltage in this region is much smaller than the other dominant parameters such as the hybridization between the STM tip and the surface (T_{dip} and $W_pk = 0.02$ eV), and the hybridization between the magnetic atoms and the metal surface ($\Gamma \geq 0.02$ eV). We believe that the non-equilibrium effect is negligibly-small in such a region. Eventually, we obtain the expression of tunneling current as:

$$\begin{aligned} I = \frac{2e}{h}\sum_\sigma \int d\omega\left(f_k - f_p\right)\Big\{ & 2\pi T_0^2\left(\Phi_{d1}^2 + \Phi_{d2}^2\right)\rho_p \Im G^r_{d1d1\sigma}(\omega) \\ & + 4\pi T_0^2 \Phi_{d1}\Phi_{d2}\rho_p \Im G^r_{d1d2\sigma}(\omega) - 2\pi^2\rho_k\rho_p W_0^2 e^{-2(z_p - R_s)/\lambda} \\ & - 4\pi T_0\left(\Phi_{d1}J_{vw}\left(r_{p1}\right) + \Phi_{d2}J_{vw}\left(r_{p2}\right)\right)\rho_p \Re G^r_{d1d1\sigma}(\omega) \\ & - 4\pi T_0\left(\Phi_{d1}J_{vw}\left(r_{p2}\right) + \Phi_{d2}J_{vw}\left(r_{p1}\right)\right)\rho_p \Re G^r_{d1d2\sigma}(\omega) \\ & - 2\pi\left(J_{vw}^2\left(r_{p1}\right) + J_{vw}^2\left(r_{p2}\right)\right)\rho_p \Im G^r_{d1d1\sigma}(\omega) \\ & - 4\pi\left(J_{vw}\left(r_{p1}\right)J_{vw}\left(r_{p2}\right)\rho_p \Im G^r_{d1d2\sigma}(\omega)\right)\Big\} \end{aligned} \tag{20}$$

Here we use the relation that $G^r_{d1d1} = G^r_{d2d2}$ and $G^r_{d1d2} = G^r_{d2d1}$ which are ensured by the symmerty of the Hamiltonian. The differential conductance (dI/dV) of the tunneling current is

$$\begin{aligned} dI/dV(V) = \frac{2e}{h}\sum_\sigma \int d\omega - \frac{\partial f_k(\omega - eV)}{\partial V}\Big\{ & 2\pi T_0^2\left(\Phi_{d1}^2 + \Phi_{d2}^2\right)\rho_p \Im G^r_{d1d1\sigma}(\omega) \\ & + 4\pi T_0^2 \Phi_{d1}\Phi_{d2}\rho_p \Im G^r_{d1d2\sigma}(\omega) - 2\pi^2\rho_k\rho_p W_0^2 e^{-2(z_p - R_s)/\lambda} \\ & - 4\pi T_0\left(\Phi_{d1}J_{vw}\left(r_{p1}\right) + \Phi_{d2}J_{vw}\left(r_{p2}\right)\right)\rho_p \Re G^r_{d1d1\sigma}(\omega) \\ & - 4\pi T_0\left(\Phi_{d1}J_{vw}\left(r_{p2}\right) + \Phi_{d2}J_{vw}\left(r_{p1}\right)\right)\rho_p \Re G^r_{12\sigma}(\omega) \\ & - 2\pi\left(J_{vw}^2\left(r_{p1}\right) + J_{vw}^2\left(r_{p2}\right)\right)\rho_p \Im G^r_{d1d1\sigma}(\omega) \\ & - 4\pi\left(J_{vw}\left(r_{p1}\right)J_{vw}\left(r_{p2}\right)\rho_p \Im G^r_{d1d2\sigma}(\omega)\right)\Big\} \end{aligned} \tag{21}$$

At $T = 0$ K, dI/dV can be rewritten in the following simplified form:

$$\begin{aligned} dI/dV(V) \propto & A_{11}\Im G^r_{d1d1\sigma}(eV) + A_{12}\Im G^r_{d1d2\sigma}(eV) \\ & + B_{11}\Re G^r_{d1d1\sigma}(eV) + B_{12}\Re G^r_{d1d2\sigma}(eV) \end{aligned} \tag{22}$$

Coefficients such as A_{11}, B_{11} can be derived from the coefficients of the Green's function in Eq. (21), i.e.,

$$\begin{aligned} A_{11} = & -2\pi T_0^2\left(\Phi_{d1}^2 + \Phi_{d2}^2\right)\rho_p, \\ & + 2\pi\left(J_{vw}^2\left(r_{p1}\right) + J_{vw}^2\left(r_{p2}\right)\right)\rho_p, \end{aligned} \tag{23}$$

$$A_{12} = -4\pi T_0^2 \Phi_{d1}\Phi_{d2}\rho_p + 4\pi J_{vw}\left(r_{p1}\right)J_{vw}\left(r_{p2}\right)\rho_p, \tag{24}$$

$$B_{11} = 4\pi T_0\left(\Phi_{d1}J_{vw}\left(r_{p1}\right) + \Phi_{d2}J_{vw}\left(r_{p2}\right)\right)\rho_p, \tag{25}$$

$$B_{12} = 4\pi T_0\left(\Phi_{d1}J_{vw}\left(r_{p2}\right) + \Phi_{d2}J_{vw}\left(r_{p1}\right)\right)\rho_p. \tag{26}$$

The third and fourth terms are related to the Fano effect and make the dI/dV spectra asymmetric. We show several values of each coefficient Eq. (22) in the case of $\Gamma = 0.022$ eV at several adatom separation in Table 1.

As can be seen from Table 1, $A_{11}\Im G^r_{11\sigma}$ is dominant and other parts play only minor roles in Eq. (22). This means that the decoupling layer suppresses the Fano effect.

2.3. Calculation of dI/dV by numerical renormalization group

To derive the imaginary and the real part of the retarded Green's function in Eqs. (21) and (22), we adopt the NRG technique [18,29–32]. We can calculate the single particle excitation spectra (SPES) by this technique. The SPES in zero-temperature is defined as

$$\begin{aligned} \rho_{di\sigma}(\omega) &= \sum_a \frac{e^{-\beta E_a}+1}{Z(T=0)}\left\{|<a|d^\dagger_{i\sigma}|g>|^2\delta(\omega - E_a) + |<a|d_{i\sigma}|g>|^2\delta(\omega + E_a)\right\} \\ &= \sum_a \frac{e^{-\beta E_a}+1}{Z(T=0)}\left\{|<a|d^\dagger_{i\sigma}|g>|^2\delta(\omega - E_a) + |<g|d^\dagger_{i\sigma}|a>|^2\delta(\omega + E_a)\right\}. \end{aligned} \tag{27}$$

The first term corresponds to electron excitations and the second term corresponds to hole excitations. $|g>$ indicates the ground states and $|a>$ indicates an excited state. E_a is the energy of the excited state. Z is the partition function. The imaginary part of the retarded Green's function is calculated from the SPES, because of the following relation:

$$\rho_{di\sigma}(\omega) = -\frac{1}{\pi}G^r_{didi}. \tag{28}$$

When the imaginary part of the retarded Green's function is calculated, we can also calculate the real part by using the Kramers–Krönig relation.

In the present study, we transform H_{A2} in Eq. (1) into two semi-infinite chains form so as to be suitable for the calculation of the SPES by NRG [19,21,22,31]:

$$\begin{aligned} H_{A2} = & \sum_{nq=\pm}\epsilon_{nq}f^\dagger_{nq}f_{nq} + \sum_{nq=\pm}\left(t_{nq}f^\dagger_{nq}f_{n+1q} + H.c.\right) \\ & + \sum_{q=\pm}E_d n_{dq} + U\sum_{i=1,2} n_{di\uparrow}n_{di\downarrow} \\ & + \sqrt{\frac{2D\Gamma}{\pi}}\sum_{q=\pm}\left(\sqrt{\gamma}f^\dagger_{0q}d_q + h.c.\right). \end{aligned} \tag{29}$$

Here, f_{nq} corresponds to the nth site of the conduction electron part of the chain (Wilson chain) with the parity q. $q = +, -$ denotes the even and odd parity states, respectively. $d_+ = \frac{d_1 + d_2}{\sqrt{2}}$ and $d_- = \frac{d_1 - d_2}{\sqrt{2}}$. D gives the conduction electron band width. ϵ_{nq} and t_{nq} are the corresponding matrix elements for the Wilson chain. When the metal surface conduction band is that for a two dimensional free electron,

$$f_{0\pm} = \int_{-D}^{D}\sqrt{\gamma_\pm(\epsilon)}c_{\epsilon\pm}\Big/\sqrt{\gamma_\pm}d\epsilon, \tag{30}$$

$$\gamma_\pm(\epsilon) = \frac{1 \pm J_0(ka)}{2}, \tag{31}$$

$$\bar{\gamma}_\pm = \int_{-D}^{D}\gamma_\pm(\epsilon)d\epsilon. \tag{32}$$

Table 1
Values of coefficients in Eq. (22) in the case of $\Gamma = 0.022$ eV at several adatom separations (a).

a (Å)	A_{11} (eV)	A_{12} (eV)	B_{11} (eV)	B_{12} (eV)
5.0	-6.6225×10^{-4}	-1.6792×10^{-9}	5.3360×10^{-7}	1.7792×10^{-7}
6.0	-6.6225×10^{-4}	6.8125×10^{-10}	5.3360×10^{-7}	6.6775×10^{-8}
7.0	-6.6225×10^{-4}	2.9035×10^{-11}	5.3360×10^{-7}	-3.5216×10^{-8}
8.0	-6.6225×10^{-4}	-4.6240×10^{-11}	5.3360×10^{-7}	-1.1929×10^{-7}
9.0	-6.6225×10^{-4}	-7.1997×10^{-11}	5.3360×10^{-7}	-1.7886×10^{-7}

The Hamiltonian H_{A2} in Eq. (29) can be viewed as a series of Hamiltonian H_{A2}^N which approaches H_{A2} in the limit of N infinite:

$$H_{A2} = \lim_{N\to\infty} \frac{2\Lambda^{(N-1)/2}\ln\Lambda}{D(1+\Lambda^{-1})} H_{A2}^N, \tag{33}$$

with

$$\begin{aligned} H_{A2}^N = \frac{2\Lambda^{(N-1)/2}\ln\Lambda}{D(1+\Lambda^{-1})}\Bigg\{ & \sum_{n,q=\pm}^{N-1}\left(t_{nq} f_{nq}^{\dagger} f_{n+1q} + H.c.\right) \\ & + \sum_{n,q=\pm}^{N} E_{nq} f_{nq}^{\dagger} f_{nq} + \sum_{q=\pm} E_d n_{dq} + U\sum_{i=1,2} n_{di\uparrow} n_{di\downarrow} \cdot \\ & + \sqrt{\frac{2D\Gamma}{\pi}} \sum_{q=\pm}\left(\sqrt{\bar{\gamma}} f_{0q}^{\dagger} d_q + h.c.\right)\Bigg\} \end{aligned} \tag{34}$$

Here Λ is the descretization factor and we set $\Lambda = 2.5$. The factor $\frac{2\Lambda^{(N-1)/2}\ln\Lambda}{D(1+\Lambda^{-1})}$ has been introduced so as to make $\frac{2\Lambda^{(N-1)/2}\ln\Lambda}{D(1+\Lambda^{-1})} t_{nq} \sim 1$ in the limit of $N\to\infty$. This H_{A2}^N satisfy the following recursive relation:

$$\begin{aligned} H_{A2}^{N+1} = \Lambda^{1/2} H_{A2}^N + \frac{2\Lambda^{N/2}\ln\Lambda}{D(1+\Lambda^{-1})}\Bigg\{ & \sum_{q=\pm} E_{N+1q} f_{N+1q}^{\dagger} f_{N+1q} \\ & + \sum_{q=\pm}\left(t_{Nq} f_{Nq}^{\dagger} f_{N+1q} + h.c.\right)\Bigg\} \end{aligned} \tag{35}$$

Repeated use of this recursive relation enables us to solve the whole Hamiltonian (H_{A2}) in Eq. (1) and calculate physical properties such as the reterded Green's function. The reterded Green's function of the transformed H_{A2} in Eq. (29) and that of the original H_{A2} in Eq. (1) keeps the following relation:

$$G_{d+d+}^r + G_{d-d-}^r = G_{d1d1}^r + G_{d2d2}^r, \tag{36}$$

$$G_{d+d+}^r - G_{d-d-}^r = G_{d1d2}^r + G_{d2d1}^r. \tag{37}$$

Thus, we can calculate the imaginary and the real part of G_{d1d1}^r and G_{d1d2}^r in Eq. (21) from the calculation results of ρ_{d+} and ρ_{d-}.

3. Numerical results and discussions

The two dominant parameters T_K and J_{RKKY} strongly depend on the value of Γ. T_K decays much faster than J_{RKKY} as Γ decreases. The values of Γ (therefore T_K) depend on the thickness, the surface condition and the type of the decoupling layer. In the present study, we set the thickness of the decoupling layer to 5Å. The experimentally estimated T_K of the magnetic atoms on a metal surface covered by a decoupling layer ranges from 2 to 6K [8,24,25]. Thus, we calculate the dI/dV spectra with $\Gamma = 0.025, 0.022$, and 0.02 eV at several adatom separations. (From Ref. [33], corresponding T_K is estimated at 6.64, 3.07,and 1.63K, respectively). In Fig. 3, we show the calculation results for the dI/dV spectra.

At $a = 5.0$ Å and $a = 9.0$ Å, there is a sharp peak structure near the Fermi level. With these adatom separations, the RKKY interaction is weak antiferromagnetic and the Kondo effect is dominant [22]. The sharp peak corresponds to the Yosida–Kondo peak. With our settings, the antiferromagnetic RKKY interaction becomes largest around $a = 7.0$ Å. As the adatom separation becomes close to 7.0 Å, the peak structure changes gradually. When $\Gamma = 0.025$ eV, the dI/dV spectra broaden as a becomes close to 7.0 Å. However, when $\Gamma = 0.022$ eV, a dip structure appears near the Fermi level. This dip structure develops to a deeper one as Γ decreases.

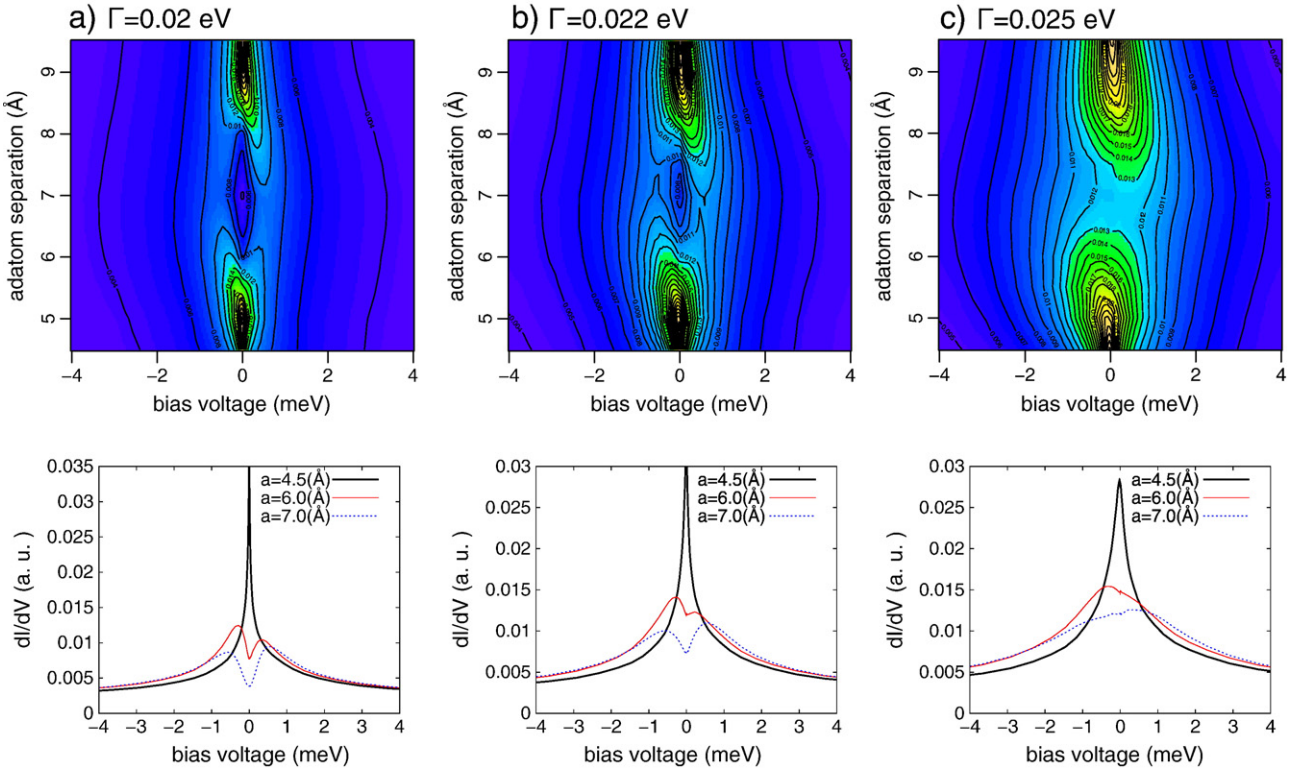

Fig. 3. dI/dV calculation results at several adatom separations with a) $\Gamma = 0.025$ eV ($T_K = 6.64$ K), b) $\Gamma = 0.022$ eV ($T_K = 3.07$ K), and c) $\Gamma = 0.02$ eV ($T_K = 1.63$ K). The STM tip is placed at $z_p = 4.0$ Å. We set $R_S = 3.0$ Å and $W_0 = T_0 = 0.02$ eV.

We find that the "parity splitting" of the single electron excitation spectra is the origin of the dip structure in the dI/dV spectra. As shown in Eq. (29), the operators in the model Hamiltonian are indexed by the parity q. Thus, the obtained physical properties such as single electron excitation spectra are divided with respect to the parity. The dI/dV spectra are proportional to the average of the single electron excitation spectra of adatom electrons on each parity channel (ρ_+,ρ_-). As shown in Fig. 4, ρ_+ and ρ_- have different peak positions. The asymmetry of the spectra results from the difference in the coupling between the adatom and conduction band in each parity channel (see Eqs. (29) and (31)). Previous studies shows that the parity splitting is one of the signatures of the smearing out of the critical point due to the breaking of the e-h symmetry [17,18]. In the present study, based on the model Hamiltonian (1), the tunneling matrix element between the localized d electrons and the metal surface conduction electrons has energy dependence, which breaks the e-h symmetry.

Another characteristic in single electron excitation spectra in each parity channel is suppression of spectra around the Fermi level when Γ is small and adatom separation becomes close to 7.0 Å. This suppression of spectra and parity splitting would induce the dip structure in observed STS spectra.

In order to investigate the electron state, we plotted the flow of low-lying many-particle energies in the NRG calculation with several adatom separations (Fig. 5).

The states are labeled by the quantum numbers total charge Q, total spin S, and total parity P. Here we show the flows of the lowest state for (Q,2S,P) = (0,0,1), (1,1,1), (−1,1,1), (1,1,−1), (−1,1,−1), (0,2,1) and (0,2,−1). The ground state is the (Q,2S,P) = (0,0,1) state. (Q,2S,P) = (±1,1,±1) states are the single electron (hole) excited states.

As shown in Fig. 5, the energy levels converge to some values for large N. Because the eigenvalues obtained in the NRG calculation are scaled (Eq. (35)), we cannot obtain information from the eigenvalues themselves in a straightforward manner. The convergence of the eigenvalues means that the Hamiltonian becomes close to the fixed point Hamiltonian of renormalization transformation [29,30,32]. Once we find the fixed point, we can extract the effective Hamiltonian which describes the electron state at the fixed point, which helps us to discuss the electr on states at 0 K. Referring [30], we define the fixed point Hamiltonian as follows:

$$H_{eff}^{N} = \Lambda^{(N-1)/2}\left\{\sum_{q=\pm,n=0}^{N-1}\eta_{qn}\left(f_{qn}^{\dagger}f_{qn+1} + H.C.\right) + K_q f_{q0}^{\dagger}f_{q0}\right\}. \tag{38}$$

$q = \pm$ is the parity index. The second term with K_q is related to the influence of potential scattering in each channel. H_{eff}^{N} is a quadratic Hamiltonian. It can hence be diagonalized exactly in terms of new operators α_{pj} such that

$$H_{eff}^{N} = \sum_{q=\pm,j=0}^{N}\xi_{qj}\alpha_{qj}^{\dagger}\alpha_{qj}. \tag{39}$$

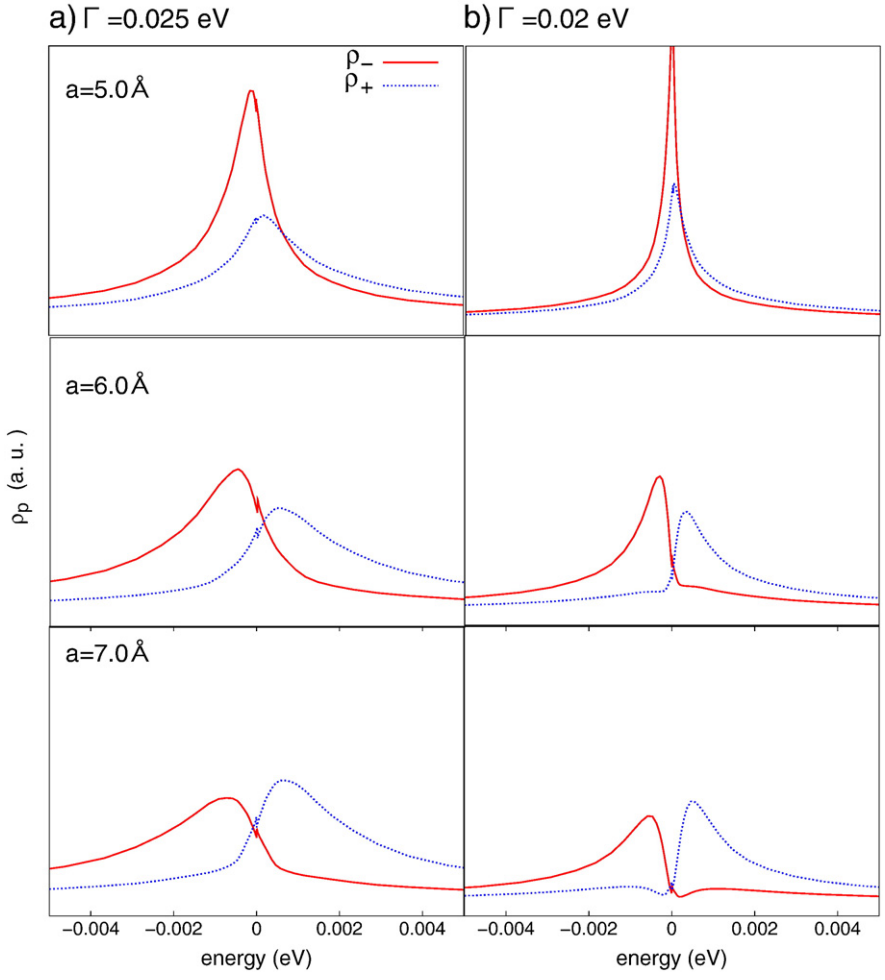

Fig. 4. Single electron excitation spectra of adatom electrons for each parity channel.

ξ_{qj} is single particle energy levels. Introducing the electron operator g_{qj} and hole operator h_{qj}, we can express H^N_{eff} for odd N as,

$$H^N_{eff} = \sum_{q=\pm,l=1}^{(N+1)/2} \eta^e_{ql} g^\dagger_{ql} g_{ql} + \eta^h_{ql} h^\dagger_{ql} h_{ql}. \tag{40}$$

Here, η^e_{ql} and η^h_{ql} are single particle levels of electron and hole, respectively.

Comparing $\eta^{e,h}_{q1}$ and the scaled energy of (Q,2S,P) = (±1,1,±1), we evaluate the value of K_q.

To clarify the discussion, we estimate the phase shift δ_q from the following relation:

$$\delta_q = -\tan^{-1}\left(\pi\rho K_q\right). \tag{41}$$

The phase shift is related to the number of electrons and holes which are virtually bound by localized spin — i.e., the phase shift is a barometer of the existence of the Kondo effect. If $\delta_\pm = \pi/2$, it means that one electron-hole pair is bound to each localized spin and quenches it individually (i.e., two Yosida–Kondo singlets are formed). On the other hand, $\delta_\pm = 0$ indicates that a localized spin–spin singlet is formed [18]. In Fig. 6, we show the result of the phase shift calculation as a function of adatom separation with several values of Γ.

The phase shift changes gradually and has an intermediate value between $\pm\pi/2$ and 0 (Fig. 6). Though the values of $\delta_\pm$ at each adatom separation are different by Γ, the change of $\delta_\pm$ is smooth in all cases. If a critical point separates the Kondo region and the antiferromagnetic region, thepossible values of $\delta_\pm$ are only 0 or $\pm\pi/2$ [18,19,34]. The intermediate value of $\delta_\pm$ would result from the crossover transition and support the conclusion that there is no critical point in the system of a magnetic dimer on a metal surface.

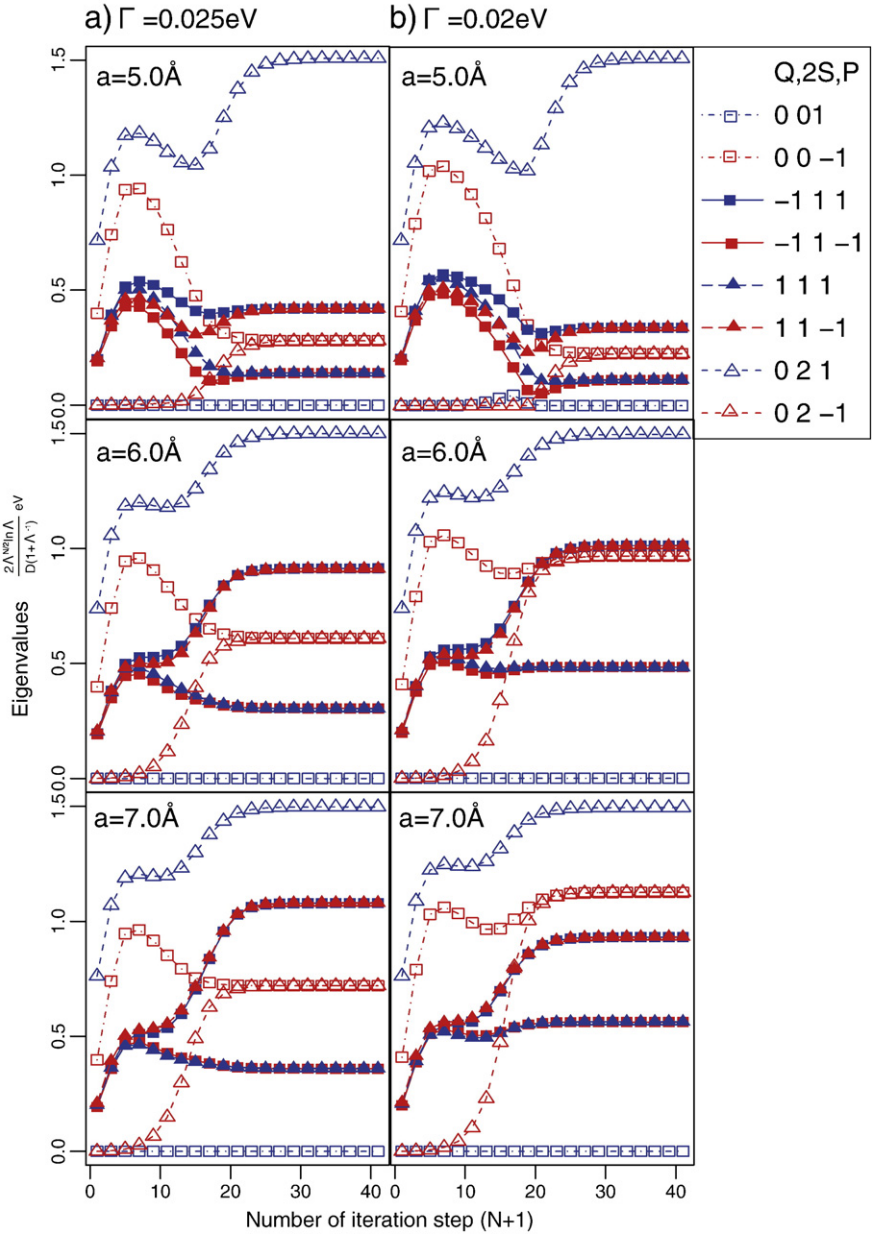

Fig. 5. Flows of the low-lying many-particle energy levels in odd iterations. $N+1$ corresponds to the iteration step number. In this calculation we calculate at $a = 5.0, 6, 0, 7, 0$ Å a) $\Gamma = 0.025$ eV b)Γ 0.02 eV. The states are labeled by the quantum numbers total charge Q, total spin S, and total parity P. The discretization factor $\Lambda = 2.5$. D = 1.0 eV.

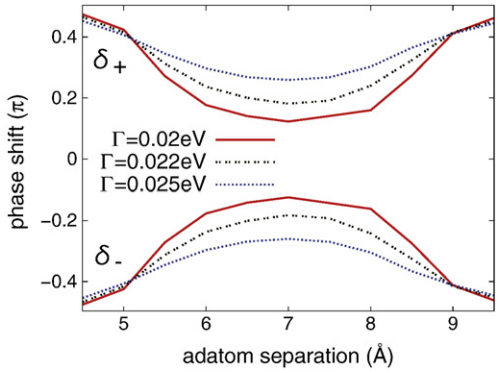

Fig. 6. Phase shift as a function of adatom separation (in units of π radians).

The smallest value of $\delta_{\pm}$ becomes close to 0 as Γ decreases. From the calculation result for the spin correlation function between adatom localized spin (Fig. 7), we conclude that the dip structure around $a = 6.0 \sim 7.0$ Å originate from the dominance of the spin–spin singlet state in the ground state.

The spin correlation is almost 0 at a = 5 Å and has quite large negative value at a = 6 ~ 7 Å. In our model, the crossover transition connects the antiferromagnetic region and the Kondo region continuously and the ground state would be the hybrid of the localized spin–spin singlet state and the Yosida–Kondo singlet state. As the antiferromagnetic correlation between the localized spins becomes large, the localized spin–spin singlet state would become dominant which induce the suppression of the excitation at the Fermi level and change of the low-lying many-particle energy levels as shown in Figs. 4 and 5.

4. Comparison with experiments

Recently, there are several STS experiments with a magnetic dimer on a surface [20,25,35,36]. Among them, we focus on the result of the magnetic dimer including Co atoms on Cu_2N/Cu(100) surface [25]. Although the bare Co atom has large spin, it is known that the ground state of Co atom on Cu_2N is a twofold degenerate ground state with $S_z = \pm 1/2$ because of the crystal field ,i.e., Co spin is reduced to an effective spin 1/2 [38,39]. Thus, the spin 1/2 model used here should well describe the experimental system. As shown in [25], when the second magnetic atom (Fe, Mn, and Co) is placed 7.2 Å apart, a deep dip appears in STS spectra. The dip width reported in Ref. [25] is around 2 mV, which is in the same order of magnitude as the dip width in Fig. 3(a). Furthermore, experimental T_K of a single Co atom on Cu_2N/Cu(100) was estimated to be around 2 K from the full width at half maximum of the Yosida–Kondo peak [24,25], which is also the same order of magnitude as the T_K in Fig. 3(a) (1.63 K). From these comparisons, we propose that the dip structure observed in STS spectra originates from the hybrid ground state between the Yosida–Kondo singlet and the localized spin–spin singlet caused by the crossover transition as discussed above.

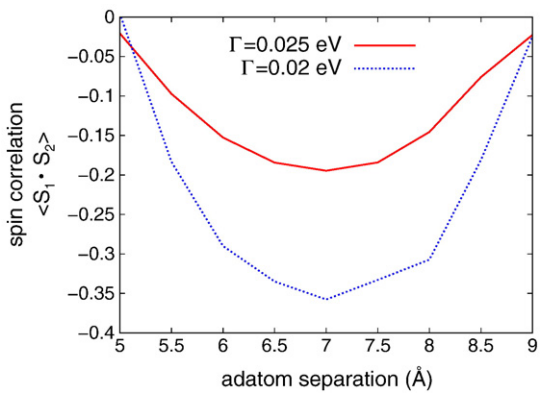

Fig. 7. Spin correlation function ($<S_1 \cdot S_2>$) as a function of adatom separation.

The dip structure in the STS spectra observed for single magnetic atoms [4–7] are of a different origin. This is mainly caused by the Fano effect [9–11,37]. Next, we show how we can distinguish between the dip resulting from the antiferromagnetic RKKY interaction (antiferromagnetic dip) and the dip resulting from the Fano effect (Fano dip) by comparing the STS spectra measured with several tip heights (z_p). In Fig. 8, we show the STS spectra of magnetic dimer on a metal surface covered by a decoupling layer when a = 7.0 Å(antiferromagnetic) and $\Gamma = 0.022$ eV. In this case, the Fano effect is suppressed by the decoupling layer. The height of the STS spectra becomes considerably decreased with increase in z_p, but, the shape of the STS spectra are almost unchanged. For comparison, we calculate the STS spectra of magnetic dimer on a bare metal surface with a = 50 Å (almost a single magnetic atom) and $\Gamma = 0.022$ eV (Fig. 9). In this case, both the height and the shape of the STS spectra are considerably changed with the increase of z_p. When $z_p = 4.0$ Å, there is a sharp peak structure near the Fermi level. However, when $z_p = 5.3$ Å, a dip structure appears near the Fermi level. The form of the dip structure at $z_p = 5.3$ Å is reminiscent of the STS spectra of the single magnetic atom in Ref. [4–7,9–11].The tip-height dependence of the antiferromagnetic dip and the Fano dip is clearly different and enables us to distinguish these two kinds of dip.

Finally, we discuss why the antiferromagnetic dip and the Fano dip have different tip-height dependence. The antiferromagnetic dip originates in the dip structure in the total SPES. On the contrary, the Fano dip is caused by the interference between the current from the STM tip to the metal surface (first-order process) and from the STM tip to the adatoms (second-order process). Whether a dip or a peak appears by the Fano effect depends on the ratio between the first-order process, the second-order process, and the interference between them. This ratio is strongly depends on the tip-height. Thus, the Fano dip only appears when the tip-height is enough large. To discuss this point in more detail, we resolve the dI/dV by the tunneling processes. In the two adatoms case, within our treatment, there are seven tunneling processes which are labeled $J1$–$J8$ in the expression of the dI/dV in Eq. (42).

$$
\begin{aligned}
dI/dV(V) = \frac{2e}{h}\sum_{\sigma}\int d\omega - \frac{\partial f_k(\omega - eV)}{\partial V} \\
\times\Big\{ & 2\pi T_0^2\left(\Phi_{d1}^2 + \Phi_{d2}^2\right)\rho_p \Im G^r_{11\sigma}(\omega) \quad (J1) \\
& + 4\pi T_0^2 \Phi_{d1}\Phi_{d2}\rho_p \Im G^r_{12\sigma}(\omega) \quad (J2) \\
& - 2\pi^2 \rho_k \rho_p W_0^2 e^{-2(z_p - R_s)/\lambda} \quad (J3) \\
& -4\pi T_0\left(\Phi_{d1} J_{vw}\left(r_{p1}\right) + \Phi_{d2} J_{vw}\left(r_{p2}\right)\right)\rho_p \Re G^r_{11\sigma}(\omega) \quad (J4) \\
& -4\pi T_0\left(\Phi_{d1} J_{vw}\left(r_{p2}\right) + \Phi_{d2} J_{vw}\left(r_{p1}\right)\right)\rho_p \Re G^r_{12\sigma}(\omega) \quad (J5) \\
& -2\pi\left(J_{vw}^2\left(r_{p1}\right) + J_{vw}^2\left(r_{p2}\right)\right)\rho_p \Im G^r_{11\sigma}(\omega) \quad (J6) \\
& -4\pi\left(J_{vw}\left(r_{p1}\right) J_{vw}\left(r_{p2}\right)\rho_p \Im G^r_{12\sigma}(\omega) \quad (J7)\right\}
\end{aligned}
\tag{42}
$$

$J1$ and $J2$ are the second-order processes. $J3$, $J6$ and $J7$ are the first-order processes. ($J3$ has no bias dependency, and we neglect $J3$ in

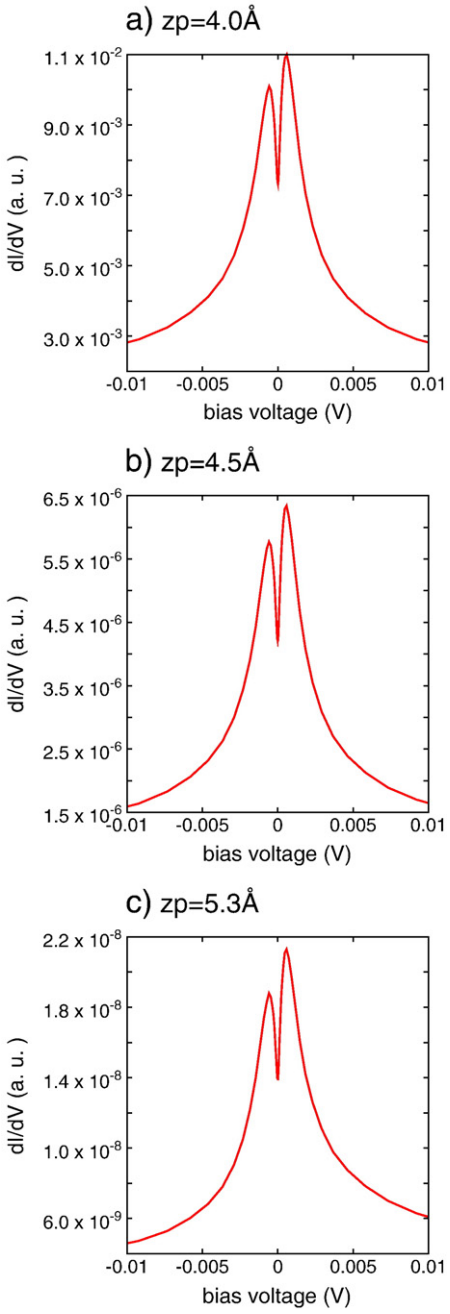

Fig. 8. dI/dV calculation results of a magnetic dimer on a metal surface covered by a decoupling layer with $a=7$ Å (antiferromagnetic) at several tip heights (z_p). a) $z_p=4.0$ Å, b) $z_p=4.5$ Å, and c) $z_p=5.3$ Å. We set $\Gamma=0.022$ eV, $R_o=5.0$ Å, and $W_0=T_0=0.02$ eV.

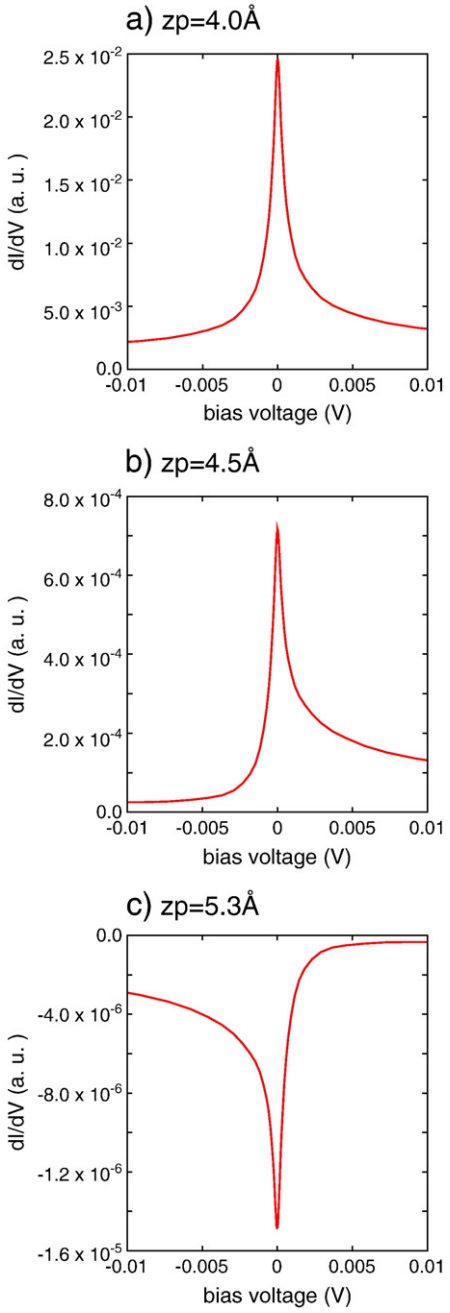

Fig. 9. dI/dV calculation results of a magnetic dimer on a bare metal surface with $a=50$ Å (almost a single magnetic atom) at several tip heights (z_p). a) $z_p=4.0$ Å, b) $z_p=4.5$ Å, and c) $z_p=5.3$ Å. We set $\Gamma=0.022$ eV, and $W_0=T_0=0.02$ eV.

the following dI/dV calculations.) $J4$ and $J5$ include both the first-order and the second-order process, and result in the Fano effect. We calculate the tunneling process-resolved dI/dV and plot the results in Figs. 10 and 11. Fig. 10 is for the two adatoms separated by 7 Å on a metal surface covered by an insulating layer (antiferromagnetic coupling) and Fig. 11 is for the two adatoms separated by 50Å on a bare metal surface (almost a single magnetic atom). In Fig. 10, $J1$ is always dominant in every tip-height. However, in Fig. 11, the dominant component switches from $J1$ to $J4$ and $J6$. $J4$ is the Fano effect term and it makes the dI/dV spectra asymmetric near the Fermi level. $J6$ originates in the current of the conduction electrons scattered by the adatoms and results in a dip around the Fermi level. The contribution from $J4$ and $J6$ makes the asymmetric dip structure, the Fano dip.

The switch of the dominant component originates in the following coefficients for each dI/dV components.

$$
\begin{aligned}
C1 &= 2\pi T_0^2\left(\Phi_{d1}^2+\Phi_{d2}^2\right)\rho_p\\
C2 &= 4\pi T_0^2\Phi_{d1}\Phi_{d2}\rho_p\\
C4 &= 4\pi T_0\left(\Phi_{d1}J_{vw}\left(r_{p1}\right)+\Phi_{d2}J_{vw}\left(r_{p2}\right)\right)\rho_p\\
C5 &= 4\pi T_0\left(\Phi_{d1}J_{vw}\left(r_{p2}\right)+\Phi_{d2}J_{vw}\left(r_{p1}\right)\right)\rho_p\\
C6 &= 2\pi\left(J_{vw}^2\left(r_{p1}\right)+J_{vw}^2\left(r_{p2}\right)\right)\rho_p\\
C7 &= 4\pi\left(J_{vw}\left(r_{p1}\right)J_{vw}\left(r_{p2}\right)\right)\rho_p
\end{aligned}
\tag{43}
$$

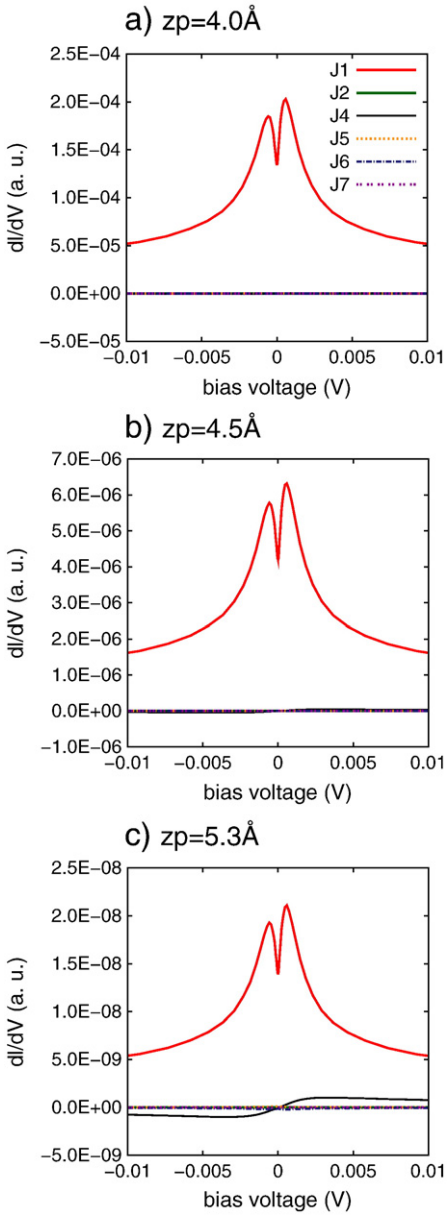

Fig. 10. Tunneling process-resolved dI/dV of a magnetic dimer on a metal surface covered by a decoupling layer with $a=7$ Å (antiferromagnetic) at several tip heights (z_p). a) $z_p=4.0$ Å, b) $z_p=4.5$ Å, and c) $z_p=5.3$ Å. We set $\Gamma=0.022$eV, $R_o=5.0$ Å, and $W_0=T_0=0.02$ eV.

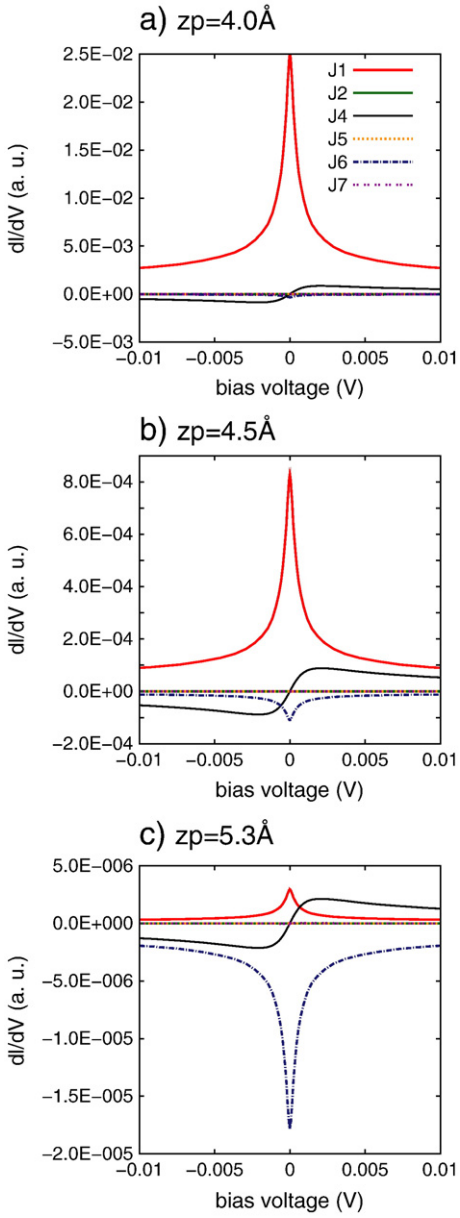

Fig. 11. Tunneling process-resolved dI/dV of a magnetic dimer on a bare metal surface with $a=50$ Å (almost a single magnetic atom) at several tip heights (z_p). a) $z_p=4.0$ Å, b) $z_p=4.5$ Å, and c) $z_p=5.3$ Å. We set $\Gamma=0.022$ eV, and $W_0=T_0=0.02$ eV.

Tables 2 and 3 are the calculation results of these coefficients for several tip heights. Table 2 is for the two adatoms separated by 7 Å on a metal surface covered by an insulating layer. (antiferromagnetic) Table 3 is for the two adatoms separated by 50 Å on a bare metal surface. (almost a single magnetic atom). As shown in Table 2, the dominant coefficient is $C1$ for all tip-height. However, in Table 3, the coefficient which has large absolute value switches from $C1$ to $C6$ and $C4$ as the tip-height increases.

To summarize, the Fano dip originates in the dip structure from scattered conduction electrons ($J6$) and the asymmetric peak from the Fano effect ($J4$). Both two components strongly depend on the tip-height on the bare metal surface. The antiferromagnetic dip is observed on the metal surface covered by the insulating layer. In such a case, the contribution of $J4$ and $J6$ is suppressed, and $J1$ becomes dominant. The antiferromagnetic dip originates in the dip in $J1$. These difference results in the different tip-height dependency between the antiferromagnetic dip and the Fano dip.

5. Conclusions

To investigate how the crossover transition between the Kondo effect dominant region and the antiferromagnetic RKKY interaction

Table 2
Values of coefficients in Eq. (43) in the case of $\Gamma=0.022$ eV and $a=7.0$ Å on a metal surface covered by an insulating layer for several tip-height (zp).The thickness of the insulating layer $R_o=5.0$ Å.$W_0=T_0=0.02$ eV.

	$z_p=4.0$Å	$z_p=4.5$Å	$z_p=5.3$Å
C1	−1.22E−5	−3.8E−7	−1.27E−9
C2	9.95E−13	3.45E−14	−1.56E−16
C4	1.09E−7	1.09E−8	2.54E−10
C5	−7.17E−9	−7.18E−10	−1.67E−11
C6	2.43E−10	7.82E−11	1.27E−11
C7	−3.19E−11	−1.03E−11	−1.68E−12

Table 3
Values of coefficients in Eq. (43) in the case of $\Gamma = 0.022$ eV and $a = 50.0$ Å on a bare metal surface for several tip-height (zp). $W_0 = T_0 = 0.02$ eV.

	zp = 4.0Å	zp = 4.5Å	zp = 5.3Å
C1	−6.62E−4	−2.19E−5	−7.79E−8
C2	0.00	0.00	0.00
C4	1.54E−4	1.59E−5	3.84E−7
C5	1.20E−6	1.24E−7	2.98E−9
C6	9.00E−6	2.90E−6	4.72E−7
C7	1.40E−7	4.50E−8	7.35E−9

dominant region can be observed through scanning tunneling spectroscopy (STS), we calculate the differential conductance (dI/dV) corresponding to STS measurements for two magnetic atoms adsorbed on a metal surface with the aid of the numerical renormalization group technique. We find that the peak structure of the dI/dV spectra changes gradually as a function of the adatom separation and the coupling (Γ) between the adatoms and the metal surface conduction band. When Γ becomes small, the peak disappears and a dip structure appears near the Fermi level. This dip structure originates from the parity splitting of the single electron excitation spectra and the manifestation of the strong antiferromagnetic correlation between the localized spins. The result of the phase shift calculation supports the conclusion that there is no critical point between the Kondo effect dominant region and the antiferromagnetic RKKY interaction dominant region but rather a crossover transition connects these regions.

In conclusion, we show that the crossover transition from the Kondo region to the antiferromagnetic region in two-impurity Kondo problem can be observed through the change of the STS spectra. In particular, the existence of the strong antiferromagnetic correlation between localized spins is observed as dip structures in the dI/dV. These findings are in good agreement with the experimental results of Otte et al. [25]. Our results indicate the possibility in STM observation of magnetic interactions on surface system with the atomic resolution, which would contribute to the realization of spintronics.

Acknowledgments

This work is supported by the Ministry of Education, Culture, Sports, Science and Technology of Japan (MEXT) through their Special Coordination Funds for the Global Center of Excellence (GCOE) program (H08) "Center of Excellence for Atomically Controlled Fabrication Technology", Grant-in-Aid for Scientific Research (C) (19510108); and the New Energy and Industrial Technology Development Organization (NEDO). E. Minamitani would like to thank the NIHON L'OREAL K.K. and Japan Society for the Promotion of Science (JSPS) for financial support and H. Matsuura (Osaka Univ.) for helpful discussions. Some of the calculations presented here were performed using the computer facilities of Cyber Media Center (Osaka University), the Institute of Solid State Physics (ISSP Super Computer Center, University of Tokyo), and the Yukawa Institute (Kyoto University).

References

[1] J. Kondo, Prog. Theor. Phys. 32 (1964) 37;
A.C. Hewson, The Kondo problem to heavy fermions, Cambridge U. P., 1993
[2] K. Yosida, Phys. Rev. 147 (1966) 223.
[3] M.F. Crommie, C.P. Lutz, D.M. Eigler, Science 262 (1993) 218.
[4] J. Li, W.-D. Schneider, R. Berndt, B. Delley, Phys. Rev. Lett. 80 (1998) 2893.
[5] V. Madhavan, W. Chen, T. Jamneala, M.F. Crommie, N.S. Wingreen, Science 280 (1998) 567.
[6] H.C. Manoharan, C.P. Lutz, D.M. Eigler, Nature (London) 403 (2000) 512.
[7] N. Knorr, M.A. Schneider, L. Diekhöner, P. Wahl, K. Kern, Phys. Rev. Lett. 88 (2002) 096804.
[8] A.J. Heinrich, J.A. Gupta, C.P. Lutz, D.M. Eigler, Science 306 (2004) 466.
[9] T. Kawasaka, H. Kasai, W.A. Diño, A. Okiji, J. Appl. Phys. 86 (1999) 6970.
[10] H. Kasai, W.A. Diño, A. Okiji, J. Electron. Spectrosc. Relat. Phenom. 109 (2000) 63.
[11] Y. Shimada, H. Kasai, H. Nakanishi, W.A. Diño, A. Okiji, Y. Hasegawa, J. Appl. Phys. 94 (2003) 334.
[12] W.A. Diño, H. Kasai, E.T. Rodulfo, M. Nishi, Thin Solid Films 509 (2006) 168.
[13] M.A. Ruderman, C. Kittel, Phys. Rev. 96 (1954) 99;
T. Kasuya, Prog. Theor. Phys. 16 (1956) 45;
K. Yosida, Phys. Rev. 106 (1957) 893.
[14] C. Jayaprakash, H.R. Krishna-murthy, J.W. Wilkins, Phys. Rev. Lett. 47 (1981) 737.
[15] B.A. Jones, C.M. Varma, J.W. Wilkins, Phys. Rev. Lett. 61 (1988) 125.
[16] B.A. Jones, C.M. Varma, Phys. Rev. B 40 (1989) 324.
[17] I. Affleck, A.W.W. Ludwig, B.A. Jones, Phys. Rev. B 52 (1995) 9528.
[18] O. Sakai, Y. Shimizu, J. Phys. Soc. Jpn 61 (1992) 2333.
[19] J.B. Silva, W.L.C. Lima, W.C. Oliveira, J.L.N. Mello, L.N. Oliveira, J.W. Wilkins, Phys. Rev. Lett. 76 (1996) 275.
[20] P. Wahl, P. Simon, L. Diekhöner, V.S. Stepanyuk, P. Bruno, M.A. Schneider, K. Kern, Phys. Rev. Lett. 98 (2007) 056601.
[21] E. Minamitani, H. Nakanishi, W.A. Diño, H. Kasai, J. Phys. Soc. Jpn 78 (2009) 084705.
[22] E. Minamitani, H. Nakanishi, W.A. Diño, H. Kasai, Solid State Commun. 149 (2009) 1241.
[23] J. Merino, L. Borda, P. Simon, Europhys. Lett. 85 (2009) 47002.
[24] A.F. Otte, M. Ternes, K.V. Bergmann, S. Loth, H. Brune, C.P. Lutz, C.F. Hirjibehedin, A.J. Heinrich, Nat. Phys. 4 (2008) 847.
[25] A.F. Otte, M. Ternes, S. Loth, C.P. Lutz, C.F. Hirjibehedin, A.J. Heinrich, Phys. Rev. Lett. 103 (2009) 107203.A.F. Otte, Ph.D. thesis, Leiden University (2008).
[26] R.E. Watson, Phys. Rev. 119 (1960) 1934.
[27] J. Rammer, H. Smith, Rev. Mod. Phys. 58 (1986) 323.
[28] H. Haug, A.P. Jauho, Quantum Kinetics in Transport and Optics of Semiconductors, Springer, Berlin, 1996.
[29] H.R. Krishna-murthy, J.W. Wilkins, K.G. Wilson, Phys. Rev. B 21 (1980) 1044.
[30] H.R. Krishna-murthy, J.W. Wilkins, K.G. Wilson, Phys. Rev. B 21 (1980) 1003.
[31] V.L. Campo Jr., L.N. Oliveira, Phys. Rev. B 72 (2005) 104432.
[32] R. Bulla, T.A. Costi, T. Pruschke, Rev. Mod. Phys. 80 (2008) 395.
[33] A. Yoshimori, H. Kasai, Solid State Commun. 58 (1986) 259.
[34] O. Sakai, Y. Shimizu, J. Phys. Soc. Jpn 61 (1992) 2348.
[35] W. Chen, T. Jamneala, V. Madhavan, M.F. Crommie, Phys. Rev. B 60 (1999) R8529.
[36] C.F. Hirjibehedin, C.P. Lutz, A.J. Heinrich, Science 312 (2006) 1021.
[37] U. Fano, Phys. Rev. 124 (1961) 1866.
[38] R. Žitko, R. Peters, Th. Pruschke, Phys. Rev. B 78 (2008) 224404.
[39] R. Žitko, R. Peters, Th. Pruschke, New J. Phys. 11 (2009) 053003.